

A PROCEDURE FOR IDENTIFYING INVASIVE WILD PARSNIP PLANTS BASED ON VISIBLE BANDS FROM UAV IMAGES

Jingyi Liu, Mohammad D Hossain and Dongmei Chen

Department of Geography and Planning, Queens University, Kingston, Canada

KEY WORDS: Wild parsnip, UAV images, pixel-based, object-based, Support Vector Machine (SVM).

ABSTRACT:

Wild parsnip is an invasive plant that has serious health risks to humans due to the toxin in its sap. Monitoring its presence has been a challenging task for conservation authorities due to its small size and irregular shape. Unmanned Aerial Vehicles (UAV) can obtain ultra-high resolution (UHR) imagery and have been used for vegetation monitoring in recent years. In this study, UAV images captured at Lemoine Point Conservation Area in Kingston, Ontario, are used to test a methodology for distinguishing wild parsnip. The objective of this study is to develop an efficient invasive wild parsnip classification workflow based on UHR digital UAV imagery. Image pre-processing flow includes image orientation, digital elevation model (DEM) and digital surface model (DSM) extractions, and orthomosaicking using Simactive's software. Three vegetation indices and three texture features are calculated and added to the mosaicked images as additional bands. Image analysis frameworks namely pixel- and object-based method and three classifiers are tested and the object-based Support Vector Machine (SVM) is selected to distinguish wild parsnip from other vegetation types. The optimal image resolutions are undertaken by comparing accuracy assessments. The results provide an executable workflow to distinguish wild parsnip and show that UAV images, with a simple digital camera, are an appropriate and economic resource for small and irregular vegetation detection. This method yields reliable and valid outcomes in detecting wild parsnip plants and demonstrates excellent performance in mapping small vegetation.

1. INTRODUCTION

Invasive plants are non-native plants to a specific region with a tendency of spreading (Boersma et al., 2006) and can change or destroy the local habitat, affect native plants, and potentially increase human and animal health risks (Paz-Kagan et al., 2019). Wild parsnip is an invasive plant that grows up to 1.5 m high with umbrella-shaped yellow flowers of diameter up to 15 cm ("Wild parsnip | Ontario.ca," 2019) (Figure 1). It can be found in large patches or a single plant. Due to its edible root, it was brought to North America by European immigrants (Zohary et al., 2012). Wild parsnip is considered toxic since it causes phytophotodermatitis (PPD), which burns the skin of both humans and animals through contact with a chemical, called furanocoumarins, in the plant's sap when the person or animal is subsequently exposed to ultra-violet radiation (Averill and DiTommaso, 2007). The affected area can remain discolored for up to two years (Carlsen and Weismann, 2007). Therefore, organizations such as the Ontario Invasive Plant Council have put greater importance on monitoring and controlling wild parsnip (Danielle and Kellie, 2014). Currently, the technique used to control the spread of wild parsnip is by eradication before flower buds have fully grown. Mowing at the wrong time will result in worsening the problem through the increased spread of the plant. However, identifying wild parsnip and monitoring its presence in a vast region has been challenging for conservation agencies due to its small size and irregular shape, especially for single scattered plants.



Figure 1. Wild parsnip and its flowers (source: <http://www.invasivespecies.com/wild-parsnip/>)

Remote sensing images acquired by satellites or airplanes have been applied for monitoring vegetation in different research areas for many years (Pande-Chhetri et al., 2017). However, traditional satellite or aircraft images cannot capture individual plant-level details, especially for scattered and small plants like a wild parsnip. Ultra-high resolution (UHR) images (sub-decimeter spatial resolution) such as Unmanned Aerial Vehicles (UAV) images have been widely applied in vegetation analysis due to the advantages of low cost, high resolution, and easier operation (Salamí et al., 2014). The UHR images captured by UAV can provide detailed features suitable for estimating the location of individual vegetation plants within several hectares (Colomina and Molina, 2014). As the flying altitude of UAV can be adjusted, the resolution of the acquired images can go up to centimeters. UAV images are usually captured by a camera which can be an inexpensive digital camera, or very expensive as with LiDAR equipment (Feng et al., 2015). Commonly, cameras used in UAVs contain only three visible bands (RGB bands) and have a limited spectral resolution. This limited spectral resolution, especially lack of infrared bands makes vegetation identification and classification more challenging.

To compensate for the absence of infrared bands, vegetation indices (VIs) and texture features calculated from RGB bands can be treated as additional bands for vegetation identification. VIs have been proven to be useful in land cover classification since 1972. Those have significantly improved the classification accuracy while analyzing satellite images (Bendig et al., 2015). The texture is another feature that analyses the homogeneity of images based on scale, uniformity, and regularity (Haralick, 1979). In recent years, texture features have been utilized in both pixel- and object-based image analysis for classifying grassland, wetland species, and forest (Dawkins and Esiobu, 2016). However, none of the previous studies examined how those ancillary features impact on the classification of scattered plants. Common image analysis methods can be categorized as pixel- and object-based. Pixel-based classification is based on spectral

properties of individual pixels and assigns each pixel to a class; whereas object-based classification groups pixels based on spectral properties, shapes, and sizes (Tarabalka et al., 2009). Both methods have some pros and cons such as the pixel-based method create a salt-and-pepper problem, do not consider neighbours and treat individual pixels as a separate entity (Pu et al., 2011). On the other hand, object-based methods require an additional step namely segmentation where it warrants user-defined inputs in grouping pixels (Liu et al., 2015). Accuracy of object-based image analysis depends on segmentation quality and feature selection for classification. Object-based image classification has shown better accuracy in many previous studies since it combines spectral and spatial features into the process (Hossain and Chen, 2019). Yet, its performance has not been tested for identifying individual plants.

The primary objective of this study was to develop an optimal workflow of classifying wild parsnip based on RGB bands of UAV imagery. This research tested the impact of spatial resolution, feature combinations, and classification methods on identifying wild parsnip during its flowering season in order to determine the optimal/ effective resolution, feature, and classification algorithms. After the testing, a workflow using an object-based classification method was proposed to map wild parsnip based on visible bands.

2. METHODS

The workflow of this study is shown in Figure 2. It can be divided into three parts: data pre-processing, image classification, optimal settings, and accuracy assessment.

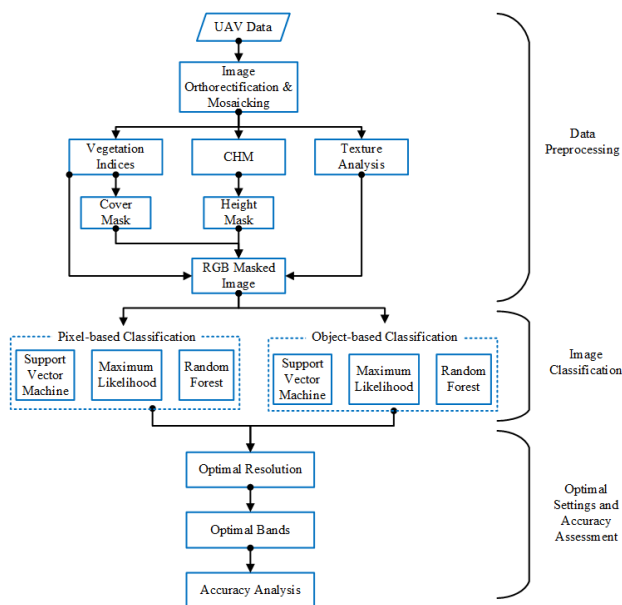


Figure 2. The workflow of distinguishing wild parsnip

Data pre-processing included image ortho-rectification, Digital Surface Model (DSM) and Digital Terrain Model (DTM) extraction, and image mosaicking. Image classification was done using both pixel- and object-based methods utilizing classifiers such as Support Vector Machine (SVM), Maximum Likelihood (ML), and Random Forest (RF) utilizing RGB bands, texture features, and vegetation indices as input variables. Canopy Height Model (CHM) was used to remove trees and tall bushes, and vegetation indices were used to identify the non-vegetation land cover. Accuracy assessment was performed using the

confusion matrix and finally, the optimal image resolution, classifier, and input variables were determined.

2.1 Data & Study Area

The study area was Lemoine Point Conservation Area, located around 44.23° N, 76.61° W, in Kingston, Ontario, Canada, and bordered by Lake Ontario and Collins Bay (Figure 3). Lemoine Point Conservation Area is a heavily used conservation area used for both recreation and natural resources and offers hiking, picnicking, cycling, and a series of outdoor activities. Wild parsnip has been found increasingly in the conservation area and is a growing concern for the Conservation Authority and Invasive Species Centre. Some places with large wild parsnip infestations were secured from access to prevent people and pets from being hurt (“Lemoine Point Conservation Area,” n.d.).

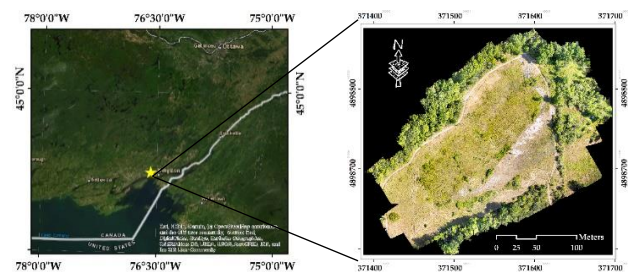


Figure 3. The location of the study area and its UAV mosaicked sample image

The Cataraqui Region Conservation Authority would like to explore the use of UAV technology to detect and locate wild parsnip and seek solutions to remove them effectively. Digital photographs were collected by a UAV operated by Kingston Aerials on July 27, 2016, for the study area (“Lemoine Point Conservation Area,” n.d.). This period coincides with the flowering season of the wild parsnip. Three-band (red, green, and blue) images were acquired with a commercial digital camera Sony A7R (Zeiss batis 25mm) at approximately 152m above terrain (received special permission from the Ministry of Transportation). The individual raw image size was 7360 pixels x 4912 pixels with a spatial resolution (GSD) of 0.94 cm per pixel and a 70% forward overlap along with a 50% side lap. The flight path was mostly parallel along with three gently banked turns to reduce the doming effects (Evers et al., 2015). This study did not utilize any ground control point for the validation of height information.

2.2 Data Pre-processing

The pre-processing procedure included image orthorectification, DSM and DTM extractions, and image mosaicking, which were all automatically processed in SimActive’s Correlator3D, a commercial photogrammetry software (Pepe and Prezioso, 2016). Correlator3D mosaicked the photos from different positions and angles and stitched the photos into a seamless image. The procedures used to mosaic the photos were based on previous tie points that were constructed between photos. According to the tie points, one of the two photos was rotated to match the other, and then the photos were stitched together. The spectral values of the mosaicked image were derived from the overlapping portions of the photos by taking the average of overlapping areas. The mosaicked image is shown in Figure 2 as well. Due to the large image size, a subset of the mosaic image (Figure 4) containing wild parsnip, trees, roads, grass, and shrubs were selected for testing the workflow and illustrating the results.

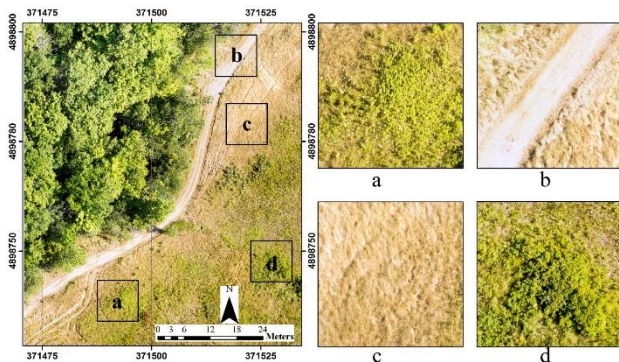


Figure 4. UAV image of the tested subset with the enlarged areas with land cover types (a) Parsnip; (b) Road; (c) Grass; (d) Shrubs

DSM is an elevation model with the top of surface objects such as buildings, vegetation, and other objects, whereas DEM represents the elevation of the bare earth without any objects. DSM and DEM have been generated in the software Correlator3D in this work. Correlator3D created a grid and calculated the correlation score for every elevation point when generating DSM. The multi-ray matching method facilitated the correlation process. The DEM was generated by applying a filtering algorithm on the DSM. The filter identified elevation points appeared higher relative to their neighbour. After removing those points, the resulting gap was filled by interpolation. CHM represents the tree and tall bushes height above the topographic surface, and values equal the DEM subtracted from the DSM. Due to the height differences between wild parsnip, and trees and part of high bushes, only pixels with the chance to grow wild parsnip remained. Based on the field survey and initial tests, pixels with CHM higher than 1.5 m were masked out as trees.

Five different land cover types were identified in the study area including wild parsnip, trees, roads, shrubs, and grass. Some flowering and other vascular plants, such as ragweed and milkweed, growing in the study area were treated as shrubs because they were not the focus of this study. Wild parsnip was showing higher spectral value in red and green bands compared to other vegetation types in the study area. For sampling, some easily recognized polygons of each land cover type were first drawn in the UAV mosaicked image by selecting the region of interest in ENVI 5.2. After the field investigation and validation, 33 training polygon samples were selected randomly for wild parsnip, and 10, 3, 19, and 24 polygon samples were selected for trees, roads, shrubs, and grass, respectively. 50% samples for each land cover type were used for the training purpose and the rest for the validation purpose. As this study used an error matrix to express classification accuracy, the multinomial distribution was utilized to determine the minimum sample size. While implementing the equation proposed by (Congalton and Green, 2008), based on field survey it was assumed that the proportion of wild parsnip would make up 10% of the map area ($\Pi_i = 10\%$), the value for B was determined from a chi-square table with 1 degree of freedom and 10% desired precision and 95% confidence interval. There were three categories ($\kappa=3$) in the classification scheme. In this study, the appropriate value of B was 5.731 and 52 total samples were required.

The spatial resolution of raw mosaicked images was 0.94 cm per pixel. One of the objectives of this study was to identify a suitable image resolution range to distinguish parsnip. The higher spatial resolution provides more detailed land cover features. However, some redundant detailed information would result in complicated processing procedures. On the other hand, the coarser image

resolution would decrease the ability to distinguish different land covers. Myint et al. (Myint et al., 2011) recommended a significantly smaller pixel size (higher resolution) than an object to identify that object in an image. They also suggested that the spatial resolution should be at least one-half of the diameter of the smallest object of interest. Therefore, the impact of image resolution on distinguishing parsnip was explored in order to identify the appropriate pixel size (or GSD) of images that can provide enough information for parsnip distinction and reduce redundant processing time. The result of this analysis would determine whether high-resolution UAV images are applicable to wild parsnip identification or not. ENVI 5.2 provided the tool that could easily adjust the image resolution defined by the user. As mentioned earlier, the average diameter of parsnip flower clusters is 15 cm, thus, the image pixels were resampled into 0.01 m, 0.02 m, 0.03 m, 0.05 m, and 0.1 m (from significantly smaller to almost the size of the object of interest) in this study.

2.3 Feature Extraction

2.3.1 VIs: Three standard VIs based on visible bands were tested for separating non-vegetated and vegetated areas. Generally, the majority of VIs commonly used in remote sensing are calculated based on visible and near-infrared bands, such as NDVI (normalized difference vegetation index). The numbers of VIs based only on visible bands are limited. Three commonly used VIs including NGBDI (Normalized Green-Blue Difference Index), EXG (Excess Green), and VEG (Vegetation) (Hague et al., 2006) were calculated using ENVI 5.2 software. The equations are listed below where G is the green band, B is the blue band, and R is the red band:

$$\text{NGBDI} = (G-B)/(G+B) \quad (1)$$

$$\text{EXG} = 2G-R-B \quad (2)$$

$$\text{VEG} = \frac{G}{R^a B^{(1-a)}} \quad \text{where } a = 0.667 \quad (3)$$

Each calculation applied to UAV images transformed a combined three-band image to a single greyscale band. In greyscale images, the values of pixels in vegetated areas show greater intensity levels than the non-vegetation area. Therefore, a threshold could be applied to vegetation indices to separate vegetation area and non-vegetation area. On the other hand, these three vegetation indices were included as separate bands for wild parsnip identification. Among the VIs, EXG was showing a higher value for wild parsnip in the higher resolution, whereas NGBDI was able to differentiate wild parsnip from other vegetation when resolution became lower. Since wild parsnip only grows in the vegetated area, non-vegetated areas could be excluded from further study. If the VIs value of a pixel was lower than the threshold, then it was placed in the non-vegetated category. Since the NGBDI band able to show the most significant differences between vegetation and non-vegetation areas (Xu et al., 2019), this study applied a threshold of 0.2 to mask out the non-vegetation areas (roads and bare grounds). Therefore, the cover mask with NGBDI larger than 0.2 was applied for further image processing.

2.3.2 Texture Features: Texture features have been applied in remote sensing for classifying vegetation types, primarily used as additional information to compensate for the lack of near-infrared band in UAV images. Second-order texture metrics based on pairs of pixels obtained from the Grey Level Co-occurrence Matrix (GLCM) are one of the commonly used metrics in features analysis (Materka and Strzelecki, 2014). Three least correlated texture features such as mean, variance, and entropy were used in this study. The GLCM was calculated

for the green band only to reduce redundancy since RGB bands were highly correlated. The equations were applied as follows:

$$\text{Entropy} = \sum_{i=0}^{G-1} \sum_{j=0}^{G-1} p(i,j) \times \log_2 [p(i,j)] \quad (4)$$

$$\text{Mean} = \sum_{i=0}^{G-1} \sum_{j=0}^{G-1} i \times p(i,j) \quad (5)$$

$$\text{Variance} = \sum_{i=0}^{G-1} \sum_{j=0}^{G-1} (i - \text{Mean})^2 \times p(i,j) \quad (6)$$

Where, G is the number of grey levels, p (i,j) is the matrix estimates of the joint probability between pairs of pixels.

The mean represents the average intensity of the texture within the image; the variance explains the variation of intensity around the mean, and the entropy describes the measure of histogram consistency. The calculation procedure for texture features is based on a moving window from pixel to pixel. Usually, the larger window size, the coarser the information obtained. The accuracy of the texture feature calculation is related to the appropriate scale that collects pixels within the same class and separates pixels from different classes. Since wild parsnip is an irregular and small object, only smaller moving window sizes (3x3, 5x5, and 7x7) were selected to test. By testing three different window sizes, a 3x3 moving window size was chosen. Although a different motion of the filter window may provide a different result, this study only applied a horizontal moving window. Texture features based on the 3x3 window size were added as ancillary bands. Among the texture features, the mean was showing a different value for wild parsnip than other vegetation.

2.4 Image Classification

2.4.1 Classification Domain: The current study implemented and compared both the pixel- and object-based classification method. Pixel-based image classification is based on the information on a single pixel, but object-based image classification is based on the information from a group of similar pixels named objects. Each object contains pixels that are homogeneous based on either texture, or sizes and shapes, or spectral information. The object-based methods require an additional step, namely segmentation to generate the object. This study utilized the region-based mean-shift segmentation method (Hossain and Chen, 2019) to generate objects. While implementing this algorithm in ArcGIS 10.6 it requires three inputs from the user such as spectral detail, spatial detail, and minimum segment size in pixels. The values used for the spectral and spatial details were 15 and 20 respectively. In addition, minimum pixels in a segment varied based on the image resolution. All the values were achieved by the trial-and-error method. The mean, standard deviation, compactness, and colour attributes were calculated for sample segments while training the classifier. On the other hand, pixel-based methods used only the statistics of an individual pixel. To make the comparison even, this study used a pixel-based accuracy matrix for both object- and pixel-based classification methods.

2.4.2 Classification Algorithm: Three classifiers were selected for identifying wild parsnips such as ML, SVM, and RF-based on their efficiency and popularity in remote sensing image analysis. The maximum likelihood algorithm is one of the most common parametric supervised classifiers and classifies each pixel/object into a class based on a Gaussian probability density function. Each pixel is assigned to the class with the highest probability value (Otukey and Blaschke, 2010). It provides a satisfactory result for normally distributed data; however, it faces difficulty in classifying non-normal distributed data. Unlike ML classifiers, the SVM (Vapnik, 1999) is a non-parametric classifier. Due to its high performance using a limited number of

reference data, SVM is widely used in remote sensing (Mountrakis et al., 2011). SVM is a complicated method compared to ML and RF since the parameters such as the kernel and its properties are all chosen by users (Gaussian Radial Basis Function kernel with Gamma value 4 was used for the current study). In this study, both ML and SVM were processed in ENVI Classic 5.2. RF has advantages of high performance on large data sets, handling abundant input variables, estimating the importance of ranking input variables, and measuring the prediction error (Rodriguez-Galiano et al., 2012). Two parameters need to be defined in the RF procedure: ntree and mtry in the calculation. Usually, the larger ntree determined, the lower out-of-bag (OOB) error generated meaning unbiased estimation of the true prediction error. Ntree was set to 1300 by trial-and-error method which provided the highest accuracy. The mtry is the number of randomly selected predictor variables. The method to calculate mtry in this algorithm is the square root of the total input variables numbers. While using RF in ArcGIS 10.6, the max tree depth and samples per class were set to 30 and 1000 respectively. Among the classifiers, RF provides a function of input variables rankings, which can be used to evaluate the contribution of different input variables to classification. The input variables included three original visible bands (red, green and blue), three vegetation indices (NGBDI, EXG, and VEG), and three texture features (mean, variance, and entropy).

3. RESULTS AND DISCUSSIONS

3.1 Pixel- Vs Object-based Classification

Pixel-based classification is widely used for low and moderate resolution images where an individual pixel contains one or more land covers. By contrast, in high-resolution images, an individual pixel contains only a portion of a land cover and neighbouring pixels contain the same land cover as well. As a result, due to ignoring the spatial relationship between pixels, the pixel-based method creates the salt and pepper problem while classifying high-resolution images (as illustrated in Figure 5). Object-based methods were recommended for analysing high-resolution images (Hay and Castilla, 2008). In identifying wild parsnip using both pixel- and object-based methods, the object-based method provided higher overall accuracy (95.29%) compared to the pixel-based method (86.45%). Although the object-based method requires an additional step of image segmentation, it warrants shorter processing time compared to the pixel-based method.

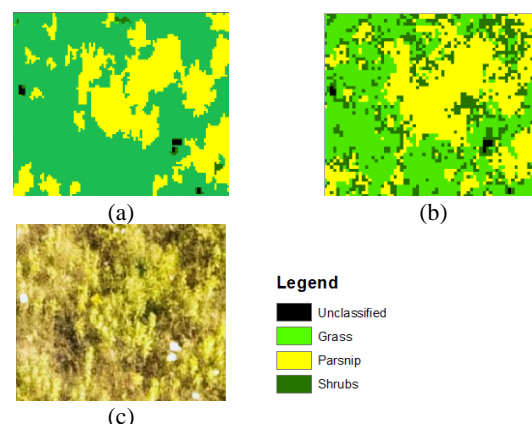


Figure 5. The Comparison between (a) object-based and (b) pixel-based classification result with (c) UAV image

3.2 Comparison of Three Classifiers

The testing procedures used RGB-only, RGB+2 (RGB plus two top-ranked features provided by RF classifier), and RGB+6 (RGB plus six features) images as input, under five different image resolutions (0.01 m, 0.02 m, 0.03 m, 0.05 m, and 0.1 m), with three different classifiers (RF, ML, and SVM). The overall accuracy under different image resolutions with different input variables by different classifiers is shown in Table 1. The masked UAV image and the classified maps from three classifiers at 0.03 m resolution (for pixel-based) and at 0.02 m (for object-based) with RGB+2 bands as input image are shown in Figure 6 and Figure 7 respectively.

Classifier	Resolution (m)	Pixel-based			Object-based		
		RGB	RGB+2	RGB+6	RGB	RGB+2	RGB+6
ML	0.01	65.5	70.2	77.5	83.0	89.2	89.6
	0.02	72.3	76.8	77.2	83.1	44.2	69.5
	0.03	66.5	72.3	74.4	81.9	53.3	77.4
	0.05	65.5	71.7	78.0	90.0	78.9	79.2
	0.1	60.9	68.2	77.7	74.9	46.8	25.0
RF	0.01	74.3	73.5	79.3	86.7	87.4	87.5
	0.02	78.2	78.6	83.1	82.7	80.0	80.5
	0.03	81.1	84.7	86.4	79.0	74.1	75.4
	0.05	77.7	80.6	80.6	74.2	76.5	77.6
	0.1	70.2	74.8	73.7	79.8	78.6	75.4
SVM	0.01	68.2	75.6	81.2	89.6	80.6	91.7
	0.02	74.3	78.5	81.0	93.7	94.8	95.3
	0.03	70.9	75.2	74.8	92.5	91.6	93.1
	0.05	69.3	73.7	78.3	93.1	93.3	94.5
	0.1	61.1	70.1	84.0	83.7	84.4	82.9

Table 1. Overall Accuracy (OA) between three classifiers under different image resolutions with different input variables

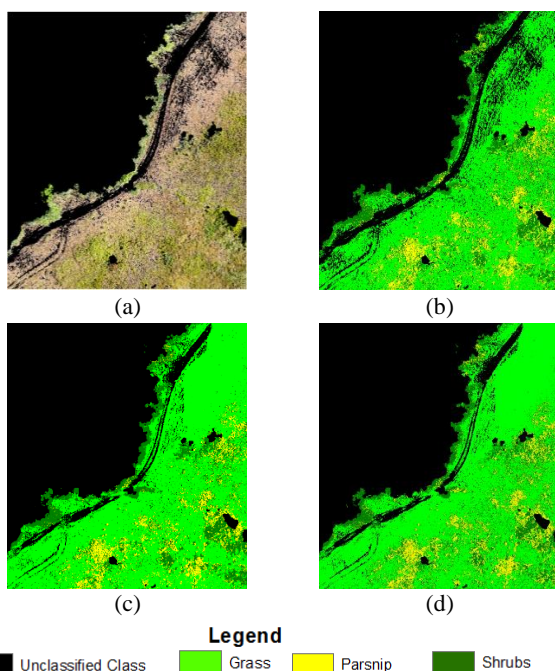


Figure 6. Pixel-based classification result: (a) UAV Masked Image (0.03 m resolution), (b) RF, (c) SVM, (d) ML

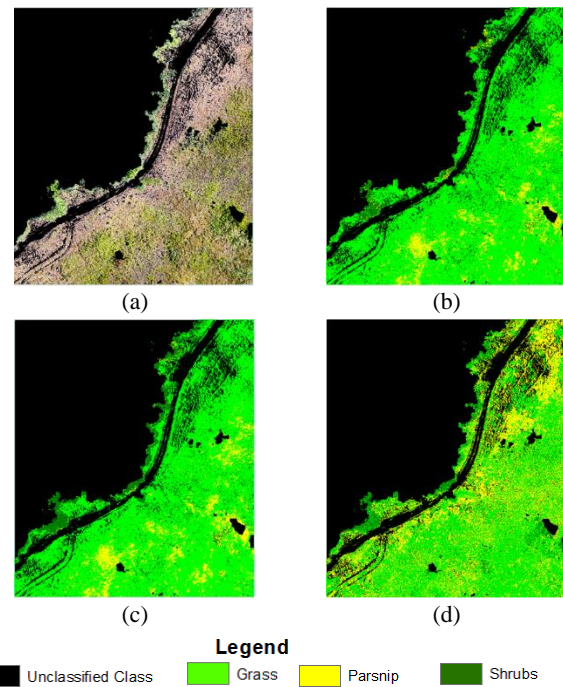


Figure 7. Object-based classification result: (a) UAV Masked Image (0.02 m resolution), (b) RF, (c) SVM, (d) ML

As Table 1 shows, random forest (RF) has achieved higher accuracy than other classifiers under the same feature inputs while using pixel-based analysis. RF has outperformed ML and SVM under the same image resolution irrespective to feature combinations and variables used. The overall accuracy was increased by 12.37% and 9.46% over ML and SVM under 0.03m RGB+2 images respectively. The highest OA was achieved under the 0.03 m RGB+6 image, and the second-highest OA was achieved at the 0.03 m RGB+2 image using RF as the classifier. ML assumes each input variable is normally distributed; however, this assumption is rarely met when analyzing real data. RF only needed several minutes to process, but SVM needed one-hour processing time. On the other hand, SVM outperformed the other two classifiers when using object-based analysis. RF also generated slightly better results in object-based analysis. ML produced an inconsistent result in different image resolution and input variables.

Since the number of wild parsnips was not the majority in the image, the visual differences on wild parsnips in the whole image were hard to see between three classification results. To illustrate classification results, one small area of the raw UAV image and three classification results using the object-based method are shown in Figure 8. The yellow parts in Figure 8(b), 8(c), and 8(d) were classified as the wild parsnip. As illustrated, the wild parsnips were distinguished well from other land covers. SVM, in particular, provided more smooth results. In Figure 8(b) and (d), wild parsnip was misclassified into grass and shrub, whereas in (c), the misclassifications of wild parsnips were decreased significantly. It is obvious that SVM classification has produced the most accurate results for wild parsnips. As demonstrated in Figure 8(c), the wild parsnips, even grown as single plants, were distinguished very well from other land covers. Some parts of shadows in the image might be misclassified into shrubs or grass, but it did not affect distinguishing wild parsnip from other land covers.

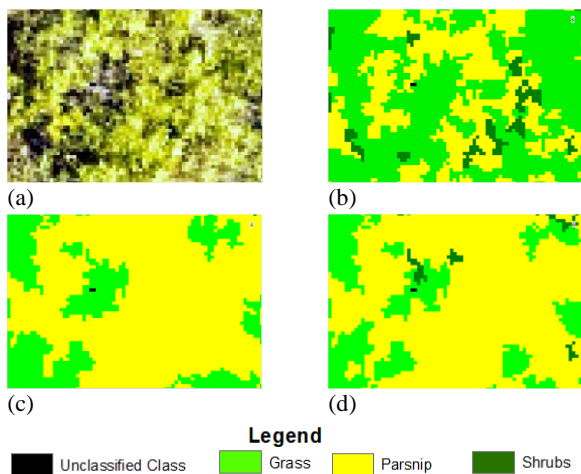


Figure 8. Detailed 0.02m RGB+2 Image Classification Results for a small subset (a) Raw UAV image, (b) ML, (c) SVM, (d) RF

3.3 The Impact of Input Variables

After selecting the best-performed classifier, the significance of the input variables was also evaluated. Since one of the objectives of this study was to find the simplest and optimal solution to distinguish wild parsnip, nine variables were considered too complicated to process in practical applications. To simplify the procedure, this study also tested the five most important variables. According to the RF variable importance rankings, each band in the RGB spectrum was always ranked in the top five, and the other two variables varied based on spatial resolution. As indicated in Figure 9(a), if image resolution was lower than 0.03 m, the most important variables were Red band, Green band, Blue band, EXG and Mean. If image resolution was equal or higher than 0.03 m (Figure 9(b)), the most important variables were the Red band, Green band, Blue band, NGBDI, and EXG. When the image resolution was lower than 0.03 m, EXG had greater importance than other variables. Mean was also crucial since the mean value could reduce the variance in the UHR image. When the image resolution was equal or bigger than 0.03m, texture features were not among the five most important variables. Therefore, besides the three original visible bands, EXG and Mean features were added as additional bands when image resolution was lower than 0.03 m; NGBDI and EXG were added as additional bands when image resolution was equal or larger than 0.03 m.

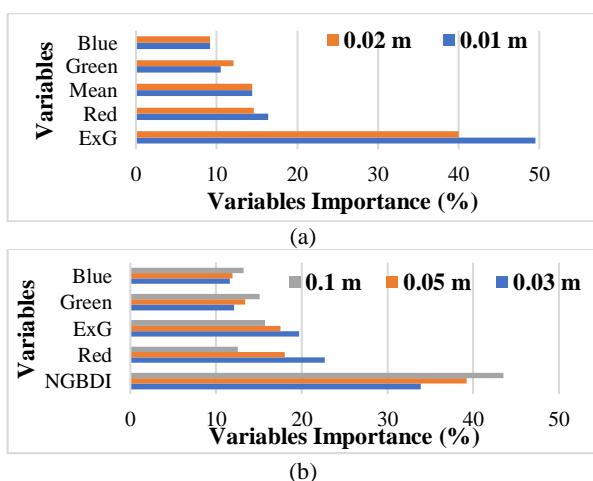


Figure 9. Input Variables Weight Comparison at image resolution of (a) 0.01m & 0.02m (b) 0.03m, 0.05m & 0.1m

The OA comparison between RGB-only, RGB+2, and RGB+6 as an input variable in object-based SVM classification is shown in Figure 10(a). In all three combinations of input variables, OA showed a similar trend when image resolution was between 0.02 m and 0.05 m. OA fall when image resolution went beyond that range. In addition, there was no significant change (<2%) in OA when additional input variables were used. Kappa value (Figure 10(b)) also demonstrated a similar pattern. Thus, this study revealed that the RGB-only input variable is sufficient for identifying wild parsnip from UAV images.

3.4 The Impact of Spatial Resolution

The impact of image resolution on classification was also examined. One advantage of UAV images is their very high spatial resolution. However, high-resolution images need more processing time because of their larger file sizes; therefore, the classification accuracy at different image resolutions was compared. As shown in Figure 9, with the different input variables used by the object-based SVM classifier, the OA reached the highest (95.29%), as well as Kappa, which reached the highest (0.93) at the image resolution of 0.02 m. Meanwhile, the OA was remaining over 90% in image resolution from 0.02 m to 0.05 m and decreased in both high and low resolution. The kappa was over 0.87 in image resolution from 0.02 m to 0.05 m and decreased to 0.75 in image resolution 0.1 m. Therefore, the optimal image resolution for distinguishing parsnip was around 0.02 m. Since wild parsnip was growing in irregular and small shapes, 0.02 m was an intermediate value for both large patches and single plants. Besides OA and kappa value, the other valuable information in the confusion matrix was user accuracy (UA) and producer accuracy (PA) of each land cover class, which are shown in Table 2-6. If only the parsnip is considered, 0.02 m resolution has the highest accuracy for both UA and PA. PA increased from 88.65% to 94.75% when the image resolution changed from 0.01 m to 0.02 m and decreased to 84.91% at image resolution 0.1 m.

	Grass	Parsnip	Shrub	Total	User's Accuracy
Grass	19635	1742	267	21644	90.72
Parsnip	540	14094	106	14740	95.62
Shrub	3354	62	18746	22162	84.59
Total	23529	15898	19119	52475	
Producer's Accuracy	83.45	88.65	98.05		OA 89.63 Kappa 0.84

Table 2. Error matrix for accuracy assessment at Image Resolution 0.01 m.

	Grass	Parsnip	Shrub	Total	User's Accuracy
Grass	5411	203	146	5760	93.94
Parsnip	133	3866	16	4015	96.29
Shrub	435	11	4757	5203	91.43
Total	5979	4080	4919	14034	
Producer's Accuracy	90.50	94.75	96.71		OA 93.70 Kappa 0.90

Table 3. Error matrix for accuracy assessment at Image Resolution 0.02 m.

	Grass	Parsnip	Shrub	Total	User's Accuracy
Grass	2288	98	58	2444	93.62
Parsnip	68	1715	1	1784	96.13
Shrub	278	0	2183	2461	88.70

Total	2634	1813	2242	6186	
Producer's Accuracy	86.86	94.59	97.37		OA 92.48 Kappa 0.89

Table 4. Error matrix for accuracy assessment at Image Resolution 0.03 m.

	Grass	Parsnip	Shrub	Total	User's Accuracy
Grass	997	67	78	1142	87.30
Parsnip	8	662	3	673	98.37
Shrub	23	0	776	799	97.12
Total	1028	729	857	2435	
Producer's Accuracy	96.98	90.81	90.55		OA 93.15 Kappa 0.90

Table 5. Error matrix for accuracy assessment at Image Resolution 0.05 m.

	Grass	Parsnip	Shrub	Total	User's Accuracy
Grass	238	28	12	278	85.61
Parsnip	20	180	24	224	80.36
Shrub	33	4	205	242	84.71
Total	291	212	241	623	
Producer's Accuracy	81.79	84.91	85.06		OA 83.74 Kappa 0.75

Table 6. Error matrix for accuracy assessment at Image Resolution 0.1 m.

4. CONCLUSIONS

This study has developed and tested a simplified object-based method to distinguish wild parsnip in vegetation fields based on UAV images. The optimal workflows for distinguishing wild parsnip from other land covers are (1) first mask out non-vegetation area and trees, and (2) then apply object-based SVM as the classifier with 0.02 m resolution image as input, which contains Red, Green, and Blue bands. This study demonstrates that UAV is an outstanding platform for vegetation monitoring and can provide accurate classification results.

The results provided an optimal and executable workflow to distinguish wild parsnip and demonstrated that UAV images are an appropriate and economic resource for small and irregular vegetation types, even equipped with a simple digital camera. This study introduced a reliable and valid method for detecting invasive wild parsnip as well as demonstrated excellent performance in mapping vegetation. This research has provided the Cataraqui Conservation Authority with a practical workflow to identify and locate wild parsnip with UAV instead of human field surveying. By implementing this workflow, the Conservation Authority can quickly identify the locations of wild parsnips and develop strategies for eliminating or controlling its spread. However, this methodology is not applicable for satellite-based images as the best resolution so far is 30 cm in WorldView4 images.

Even though the workflow performed well, the approach still has some limitations. The first is related to the segmentation algorithm. This study applied only the mean-shift algorithm to generate segments. However, other algorithms such as a multiresolution or hybrid method may generate a better result. Secondly, land cover types in this UAV acquired area did not contain other yellow flowering types of vegetation. This workflow may not be suitable for distinguishing wild parsnip

from other similar-sized plants with yellow flowers. Future study will be to test the workflow identified through this research with images that contain another similar-sized yellow flowering plant. Thirdly, this study used pixel values instead of reflectance for the analysis which is a common practice in analysing UAV images. However, the reflectance may provide better accuracy and will assist in implementing this methodology for multi-temporal studies. Thus, our future study will utilize reflectance instead of the pixel value.

ACKNOWLEDGMENT

This research was supported by Queen's graduate scholarship and NSERC Discovery grant. The authors would like to thank Cataraqui Conservation Authority to provide us the UAV images and help on validating field data.

REFERENCES

- Averill, K.M., DiTommaso, A., 2007. Wild Parsnip (*Pastinaca sativa*): A Troublesome Species of Increasing Concern. *Weed Technol.* 21, 279–287. doi.org/10.1614/WT-05-186.1
- Bendig, J., Yu, K., Aasen, H., Bolten, A., Bennertz, S., Broscheit, J., Gnyp, M.L., Bareth, G., 2015. Combining UAV-based plant height from crop surface models, visible, and near infrared vegetation indices for biomass monitoring in barley. *Int. J. Appl. Earth Obs. Geoinf.* 39, 79–87. doi.org/10.1016/j.jag.2015.02.012
- Boersma, P.D., Reichard, S.H., Van Buren, A.N., 2006. *Invasive Species in the Pacific Northwest*. University of Washington Press. doi.org/10.1007/s10530-007-9108-y
- Breiman, L., 2001. Random Forests. *Mach. Learn.* 45, 5–32. doi.org/10.1023/A:1010933404324
- Carlsen, K., Weismann, K., 2007. Phytophotodermatitis in 19 children admitted to hospital and their differential diagnoses: Child abuse and herpes simplex virus infection. *J. Am. Acad. Dermatol.* 57, S88–S91. doi.org/10.1016/j.jaad.2006.08.034
- Colomina, I., Molina, P., 2014. Unmanned aerial systems for photogrammetry and remote sensing: A review. *ISPRS J. Photogramm. Remote Sens.* 92, 79–97. doi.org/10.1016/j.isprsjprs.2014.02.013
- Congalton, R.G., Green, K., 2008. *Assessing the accuracy of remotely sensed data: principles and practices*, Second. ed. CRC Press.
- Conrad, C., Fritsch, S., Zeidler, J., Rucker, G., Dech, S., 2010. Per-Field Irrigated Crop Classification in Arid Central Asia Using SPOT and ASTER Data. *Remote Sens.* 2, 1035–1056. doi.org/10.3390/rs2041035
- Danielle, T., Kellie, S., 2014. Invasive Wild Parsnip (*Pastinaca sativa*) Best Management Practices in Ontario Ontario Invasive Plant Council [WWW Document]. Ontario Invasive Plant Council. URL http://www.ontarioinvasiveplants.ca/wp-content/uploads/2016/07/OIPC_BMP_WildParsnip_Feb182014_FINAL2.pdf (accessed 5.1.18).
- Dawkins, K., Esiobu, N., 2016. Emerging Insights on Brazilian Pepper Tree (*Schinus terebinthifolius*) Invasion: The Potential Role of Soil Microorganisms. *Front. Plant Sci.* 7, 712. doi.org/10.3389/fpls.2016.00712

- Evers, L., Barros, A.I., Monsuur, H., Wagelmans, A., 2015. UAV Mission Planning: From Robust to Agile, in: Zeimpekis, V., Kaimakamis, G., Daras, N.J. (Eds.), *Military Logistics: Research Advances and Future Trends*. Springer International Publishing, Cham, pp. 1–17. doi.org/10.1007/978-3-319-12075-1_1
- Feng, Q., Liu, J., Gong, J., 2015. UAV Remote Sensing for Urban Vegetation Mapping Using Random Forest and Texture Analysis. *Remote Sens.* 7, 1074–1094. doi.org/10.3390/rs70101074
- Hague, T., Tillett, N.D., Wheeler, H., 2006. Automated Crop and Weed Monitoring in Widely Spaced Cereals. *Precis. Agric.* 7, 21–32. doi.org/10.1007/s11119-005-6787-1
- Haralick, R.M., 1979. Statistical and structural approaches to texture. *Proc. IEEE* 67, 786–804. doi.org/10.1109/PROC.1979.11328
- Hay, G J, Castilla, G., 2008. Geographic Object-Based Image Analysis (GEOBIA): A new name for a new discipline, in: Blaschke, T., Lang, S., Hay, Geoffrey J. (Eds.), *Object-Based Image Analysis: Spatial Concepts for Knowledge-Driven Remote Sensing Applications*. Springer Science & Business Media, pp. 75–90.
- Hossain, M.D., Chen, D., 2019. Segmentation for Object-Based Image Analysis (OBIA): A review of algorithms and challenges from remote sensing perspective. *ISPRS J. Photogramm. Remote Sens.* 150, 115–134. doi.org/10.1016/j.isprsjprs.2019.02.009
- Lemoine Point Conservation Area [WWW Document], n.d. . Cataraqui Reg. Conserv. Auth. URL <https://crca.ca/conservation-lands/conservation-areas/lemoine-point-conservation-area/> (accessed 5.1.18).
- Liu, J., Li, P., Wang, X., 2015. A new segmentation method for very high resolution imagery using spectral and morphological information. *ISPRS J. Photogramm. Remote Sens.* 101, 145–162. doi.org/10.1016/j.isprsjprs.2014.11.009
- Martin, F.-M., Müllerová, J., Borgniet, L., Dommanget, F., Breton, V., Evette, A., 2018. Using Single- and Multi-Date UAV and Satellite Imagery to Accurately Monitor Invasive Knotweed Species. *Remote Sens.* 10, 1662. doi.org/10.3390/rs10101662
- Materka, A., Strzelecki, M., 2014. *Texture Analysis Methods—A Review*. Brussels.
- Mountrakis, G., Im, J., Ogole, C., 2011. Support vector machines in remote sensing: A review. *ISPRS J. Photogramm. Remote Sens.* 66, 247–259. doi.org/10.1016/j.isprsjprs.2010.11.001
- Müllerová, J., Brůna, J., Dvořák, P., Bartaloš, T., Vítková, M., 2016. Does the data resolution/origin matters? Satellite, airborne and UAV imagery to tackle plant invasions. *Int. Arch. Photogramm. Remote Sens. Spat. Inf. Sci.* 41, 903–908. doi.org/10.5194/isprsarchives-XLI-B7-903-2016
- Myint, S.W., Gober, P., Brazel, A., Grossman-Clarke, S., Weng, Q., 2011. Per-pixel vs. object-based classification of urban land cover extraction using high spatial resolution imagery. *Remote Sens. Environ.* 115, 1145–1161. doi.org/10.1016/j.rse.2010.12.017
- Otukei, J.R., Blaschke, T., 2010. Land cover change assessment using decision trees, support vector machines and maximum likelihood classification algorithms. *Int. J. Appl. Earth Obs. Geoinf.* 12, S27–S31. doi.org/10.1016/J.JAG.2009.11.002
- Pande-Chhetri, R., Abd-Elrahman, A., Liu, T., Morton, J., Wilhelm, V.L., 2017. Object-based classification of wetland vegetation using very high-resolution unmanned air system imagery. *Eur. J. Remote Sens.* 50, 564–576. doi.org/10.1080/22797254.2017.1373602
- Paz-Kagan, T., Silver, M., Panov, N., Karnieli, A., 2019. Multispectral Approach for Identifying Invasive Plant Species Based on Flowering Phenology Characteristics. *Remote Sens.* 11, 953. doi.org/10.3390/rs11080953
- Pepe, M., Fregonese, L., Scaioni, M., 2018. Planning airborne photogrammetry and remote-sensing missions with modern platforms and sensors. *Eur. J. Remote Sens.* 51, 412–435. doi.org/10.1080/22797254.2018.1444945
- Pepe, M., Prezioso, G., 2016. Two Approaches for Dense DSM Generation from Aerial Digital, in: 2nd International Conference on Geographical Information Systems Theory, Applications and Management (GISTAM 2016). pp. 63–70.
- Pu, R., Landry, S., Yu, Q., 2011. Object-based urban detailed land cover classification with high spatial resolution IKONOS imagery. *Int. J. Remote Sens.* 32, 3285–3308. doi.org/10.1080/01431161003745657
- Rodriguez-Galiano, V.F., Chica-Olmo, M., Abarca-Hernandez, F., Atkinson, P.M., Jeganathan, C., 2012. Random Forest classification of Mediterranean land cover using multi-seasonal imagery and multi-seasonal texture. *Remote Sens. Environ.* 121, 93–107. doi.org/10.1016/J.RSE.2011.12.003
- Salamí, E., Barrado, C., Pastor, E., 2014. UAV Flight Experiments Applied to the Remote Sensing of Vegetated Areas. *Remote Sens.* 6, 11051–11081. doi.org/10.3390/rs61111051
- Som-ard, J., Hossain, M.D., Ninsawat, S., Veerachitt, V., 2018. Pre-harvest Sugarcane Yield Estimation Using UAV-Based RGB Images and Ground Observation. *Sugar Tech.* doi.org/10.1007/s12355-018-0601-7
- Tarabalka, Y., Benediktsson, J.A., Chanussot, J., 2009. Spectral–Spatial Classification of Hyperspectral Imagery Based on Partitional Clustering Techniques. *IEEE Trans. Geosci. Remote Sens.* 47, 2973–2987. doi.org/10.1109/TGRS.2009.2016214
- Torres-Sánchez, J., López-Granados, F., Peña, J.M., 2015. An automatic object-based method for optimal thresholding in UAV images: Application for vegetation detection in herbaceous crops. *Comput. Electron. Agric.* 114, 43–52. doi.org/10.1016/J.COMPAG.2015.03.019
- Vapnik, V.N., 1999. An overview of statistical learning theory. *IEEE Trans. Neural Networks.* 10, 988–999. doi.org/10.1109/72.788640
- Wild parsnip | Ontario.ca [WWW Document], 2019. Minist. Nat. Resour. For. URL <https://www.ontario.ca/page/wild-parsnip> (accessed 7.30.19).
- Xu, J., Gu, H., Meng, Q., Cheng, J., Liu, Y., Jiang, P., Sheng, J., Deng, J., Bai, X., 2019. Spatial pattern analysis of Haloxylon ammodendron using UAV imagery - A case study in the

Gurbantunggut Desert. *Int. J. Appl. Earth Obs. Geoinf.* 83, 101891. doi.org/10.1016/j.jag.2019.06.001

Zohary, D., Hopf, M., Weiss, E., 2012. Domestication of Plants in the Old World: *The origin and spread of domesticated plants in Southwest Asia, Europe, and the Mediterranean Basin*. Oxford University Press.